

Ocean Dynamics

Turbulent high-latitude oceanic intrusions - details of on-smooth apparent isopycnal transport West of Svalbard --Manuscript Draft--

Manuscript Number:	ODYN-D-16-00014
Full Title:	Turbulent high-latitude oceanic intrusions - details of on-smooth apparent isopycnal transport West of Svalbard
Article Type:	Original Papers
Keywords:	high-resolution temperature observations; West-Svalbard; poleward of critical lunar tidal latitude; intrusions; high-frequency internal wave breaking; non-smooth isopycnal dispersal
Abstract:	<p>Filament intrusions are observed in high-resolution temperature (T-) measurements from a 100-m and several months-long mooring in the Fram Strait around 400 m water depth at the continental slope West of Svalbard (Spitsbergen, Norway). In this dynamic environment, a wide variety of intrusive layers are observed with thicknesses between 5 and 80 m with warmer water between cooler waters above and below. The layers typically last from several hours up to one day, exceeding the local buoyancy period but not lasting as long as intrusive layers in the open ocean. The intrusions are a result of an interminglement of Arctic and North-Atlantic waters and generated in the basins interior and locally via internal wave steepening upon the sloping bottom. Freely propagating semidiurnal lunar internal tides cannot exist without background vorticity at these high-latitudes. Strongly nonlinear turbulent bores are not observed at the tidal periodicity, but wave fronts occur at the sub-inertial frequency of dominant baroclinic instability. The fronts are in part associated with near-buoyancy frequency internal waves (breaking). The details of the moored T-observations and their spectral content demonstrate the non-smooth, relatively turbulent development including convective overturning and shear-induced instabilities when intrusions disperse in presumably salinity-compensated isopycnal layers. Some effects of this 'isopycnal mixing' or 'mixing while intruding' on the dispersal of materials and different water masses is discussed.</p>

1
2
3
4
5
6
7
8
9
10
11
12
13
14
15
16
17
18
19
20
21
22
23
24
25
26
27
28
29
30
31
32
33
34
35
36
37
38
39
40
41
42
43
44
45
46
47
48
49
50
51
52
53
54
55
56
57
58
59
60
61
62
63
64
65

Turbulent high-latitude oceanic intrusions – details of non-smooth apparent isopycnal transport West of Svalbard

by Hans van Haren^{a,*}, Jens Greinert^{b,c,d}

^aNIOZ Royal Netherlands Institute for Sea Research and Utrecht University, P.O. Box 59, 1790 AB Den Burg, the Netherlands.

*e-mail: hans.van.haren@nioz.nl

^bGEOMAR Helmholtz Centre for Ocean Research Kiel Wischhofstrasse 1-3, 24148 Kiel, Germany.

^cChristianAlbrechts University, Institute of Geosciences, Ludewig-Meyn-Str. 10, 24118 Kiel, Germany.

^dCAGE – Centre for Arctic Gas Hydrate, Environment and Climate, UiT The Arctic University of Norway, Tromsø, Norway.

37 **Abstract**

1
2 38 Filament intrusions are observed in high-resolution temperature (T-) measurements from a 100-m and
3
4 39 several months-long mooring in the Fram Strait around 400 m water depth at the continental slope
5
6 40 West of Svalbard (Spitsbergen, Norway). In this dynamic environment, a wide variety of intrusive
7
8 41 layers are observed with thicknesses between 5 and 80 m with warmer water between cooler waters
9
10 42 above and below. The layers typically last from several hours up to one day, exceeding the local
11
12 43 buoyancy period but not lasting as long as intrusive layers in the open ocean. The intrusions are a
13
14 44 result of an interminglement of Arctic and North-Atlantic waters and generated in the basins interior
15
16 45 and locally via internal wave steepening upon the sloping bottom. Freely propagating semidiurnal
17
18 46 lunar internal tides cannot exist without background vorticity at these high-latitudes. Strongly
19
20 47 nonlinear turbulent bores are not observed at the tidal periodicity, but wave fronts occur at the sub-
21
22 48 inertial frequency of dominant baroclinic instability. The fronts are in part associated with near-
23
24 49 buoyancy frequency internal waves (breaking). The details of the moored T-observations and their
25
26 50 spectral content demonstrate the non-smooth, relatively turbulent development including convective
27
28 51 overturning and shear-induced instabilities when intrusions disperse in presumably salinity-
29
30 52 compensated isopycnal layers. ~~Some effects of this ‘isopycnal mixing’ or ‘mixing while intruding’ on~~
31
32 53 ~~the dispersal of materials and different water masses is discussed.~~
33
34
35
36
37
38
39

40 55 **Keywords** high-resolution temperature observations; West-Svalbard; poleward of critical
41
42 56 lunar tidal latitude; intrusions; high-frequency internal wave breaking; non-smooth isopycnal
43
44 57 dispersal
45
46
47
48
49
50
51
52
53
54
55
56
57
58
59

1 Introduction

In the ocean, density compensation of temperature by salinity variations is often found in the vertically quasi-homogeneous ‘mixed-layer’ near the surface (e.g., Rudnick and Ferrari 1999). In deeper waters, density variations are generally dominated by temperature variations (Schmitt 1999), with exceptions, e.g., around the relatively warm and salty Mediterranean outflow lenses ‘Meddies’ in the North-Atlantic Ocean (Hebert et al. 1990; Ruddick 1992) and the relatively warm and salty North-Atlantic waters colliding with Arctic waters around Spitsbergen (Perkin and Lewis 1984). In general, the associated filaments of intruding water with distinctly different characteristics than waters above and below can be followed across 100 km or more in the open ocean (May and Kelley 2001) or last for months (Hebert et al. 1990). This occurs in deep ocean waters as well as in shallow seas like the Baltic (Holtermann 2015). With the dispersing and eventually disappearing intrusions, other (conservative) suspended and soluble materials that further characterize the different water masses become integrated in the (Atlantic) ocean circulation.

~~For the~~ main driver of these ‘thermohaline intrusions’, double diffusive fluxes have been suggested. As described by Turner (1979), a layer of warm and salty water may intrude at its particular density level in a stably density stratified ocean with relatively cooler and fresher characteristics due to salt finger diffusion at its lower edge and diffusive convection at its upper edge. This is because of the higher (molecular) diffusivity for heat compared with salinity, thus causing growing instabilities for the lower edge and restoring oscillatory motions for the upper edge. According to Ruddick (1984; 1992), the particular baroclinic instability generates different slopes of intrusions on either side of a front, initially separating two different water masses after equalizing (homogenizing) density differences.

As the turbulent mixing associated with the homogenization can be particularly large above sloping topography (Armi 1978), it has been suggested that these intrusions may largely transport mixed waters from the near-bottom ‘boundary layers’ into the ocean interior. Such topography-induced intrusions are a plausible explanation for the generation of so-called ‘nepheloid layers’ of sediment whirled up from sloping bottoms and transported more or less along isopycnals into the

1
2 87 interior (Cacchione and Drake 1986), but not necessarily above ‘critical slopes for internal tidal
3 88 waves’ (Hosegood and van Haren 2004; the present data).

4 89 Here, we hypothesize that these layers extending from sloping topography must be different from
5
6 90 ‘water mass intrusions’ associated with e.g. Meddies. This is because the main turbulent mixing agent
7
8 91 above sloping topography is the breaking of baroclinic (‘internal’) waves, generally through bores
9
10 92 occurring once or twice at the dominant tidal, inertial but also sub-inertial periodicities (Hosegood and
11
12 93 van Haren 2004). The highly nonlinearly deformed waves transforming into upslope propagating
13
14 94 bores induce so much turbulent mixing that is estimated by van Haren and Gostiaux (2012) to be
15
16 95 sufficient to maintain the ocean interior stratified as it governs the transport of heat downwards (Munk
17
18 96 1966). Although the sloping topography induces rapid re-stratification, after the turbulent overturning,
19
20 97 and to within about a meter from the bottom, the thus effective mixing is expected to also destroy
21
22 98 intrusions by homogenizing the near-bottom region periodically for brief moments. Associated
23
24 99 intrusions are not thought to exist longer than, e.g., a tidal period. This hypothesis is investigated in a
25
26
27
28
29 100 study that also aims to reveal in some detail the character of intrusions.

30
31 101 For this purpose, high-resolution temperature sensors were moored for a year above the continental
32
33 102 slope on the east side of the arctic Fram Strait, in an area where ~~also~~ methane seeps are active. Similar
34
35 103 observations have been made in the Southern Ocean in 950 m water depth at the continental slope off
36
37 104 New Zealand (van Haren and Greinert 2013). There, 20-50 m thick temperature inversions were
38
39 105 observed persistent for 1-24 h, but the recorded data set was rather short in time (9 days) for extensive
40
41 106 study of the origin of the intrusions. The observations offshore New Zealand were made in an area of
42
43 107 active methane seepage with gas bubble release to investigate if such release has a measurable impact
44
45 108 on the ocean stratification. Although gas release was found in the area, the turbulent mixing was not
46
47 109 due to bubble rising effects but could be related to sloping boundary layer effects as large internal
48
49 110 wave breaking through nonlinear bores was observed. Such wave breaking may lead to intrusions, as
50
51 111 is investigated here.

52
53
54
55 112 Intrusions are easily detected in moored thermistor string data when their duration surpasses that of
56
57 113 the local buoyancy period. As no moorable salinity sensors were available, quantification of
58
59 114 turbulence parameter estimates cannot be made when intrusions are regularly present.

115

2 Materials, background conditions and methods

A taut-wire mooring was deployed from 25 July 2012 to 16 July 2013 at the continental slope West of Svalbard (Spitsbergen, Norway; Fig. 1). Its position was $78^{\circ} 37.09'N$, $9^{\circ} 19.00'E$, $H = 450$ m water depth. It was thus about 4° poleward of the latitude at which the local inertial frequency ‘critically’ matches the semidiurnal lunar tidal frequency M_2 . As a result, no freely propagating internal waves at the dominant tidal frequency can exist at the present mooring site without the aid of negative relative vorticity, e.g., generated by mesoscale eddies. Internal tides, if existent, thus vary between trapped and propagating modes at sub-inertial periodicities.

A total of 100 ‘NIOZ4’ self-contained temperature (T) sensors were taped at 1.0 m vertical intervals to a nylon-coated steel cable, with the lowest sensor 6.4 m above the bottom and the upper about 2.5 m below a single elliptic floatation providing 2000 N of net buoyancy. NIOZ4 is an upgrade of NIOZ3 (van Haren et al. 2009), with similar characteristics, except for its **reduced size** (2/3 smaller). The sensors sampled at a rate of 1 Hz, with precision better than $0.001^{\circ}C$ and a noise level of about $6 \times 10^{-5}^{\circ}C$. They were synchronized to a **standard clock** via induction every 6 h, so that the timing mismatch was less than 0.04 s. Due to battery problems, only half of the sensors completed the one year record of the duration of the mooring. Here, the focus is on the first 100 days when most sensors were operational.

No current meters were moored and we have to refer to previous current observations (e.g., Kasajima and Svendsen 2002; Teigen et al. 2011). From the historic observations obtained in the vicinity of our mooring site it is learned that currents are largely barotropic, with little phase shifts in the vertical, especially for diurnal and semidiurnal tides (station F, Fig. 2 in Kasajima and Svendsen 2002). The semidiurnal current is mainly directed along the shelf (Teigen et al. 2011). Largest currents are found at sub-inertial frequencies, due to meanders or eddies (Schauer et al. 2004), that are considered generated through 35-75 h baroclinic instabilities slightly off-shelf (Teigen et al. 2011).

During the mooring handling cruises, shipborne SeaBird-9plus Conductivity-Temperature-Depth (CTD) data were obtained within 1 km from the mooring site. These data are used to establish the

142 temperature-density relationship around the depth of the moored temperature sensors. Data from the
143 latter are first transferred to Conservative Temperature (Θ) values (IOC, SCOR, IAPSO, 2010),
144 before they are used as an estimate for (variations in) potential density anomaly referenced to a level
145 of 400 dBar ($\sigma_{0.4}$) following a not very tight, constant linear relationship obtained from CTD data
(Figure 2), $\delta\sigma_{0.4} = \alpha\delta\Theta$, $\alpha = -0.067\pm 0.01 \text{ kg m}^{-3}\text{C}^{-1}$ denoting the thermal expansion coefficient under
147 local conditions. This relationship is the mean for the lower 150 m of the CTD-profile.

148 Like turbulence parameter estimates, local values for buoyancy frequency N can also not be
149 established as reordering the moored temperature (density) profiles in statically stable ones has no
150 meaning when (numerous) intrusions are present. Only a sufficiently long and full-vertical-range
151 mean N -value can be estimated using the present data, and which is compared with N from CTD-data.

153 3 Observations

154 3.1 Overview

155 Hydrographically, the CTD-data from the single station at 1 km to the southwest of the mooring
156 show that between 50 and 250 m temperature dominates over salinity contributions to density (Fig.
157 3a-c). Even in this layer small intrusions do occur, e.g. near -170 m. Above this layer, in the upper 20
158 m from the surface, the water is more or less well mixed and relatively low in salinity. Below this
159 well-mixed surface layer down to about 400 m, temperature and salinity roughly compensate each
160 other, although temperature variations still gain so that density is stably stratified. A range of about 50
161 m above the bottom is near-homogeneous albeit with weakly stratified portions, in this CTD-profile.
162 As will be shown below, this near-bottom range varies strongly with time. Over a five day period, the
163 mean Conservative Temperature change over a 100 m vertical range (of the moored T-sensors)
164 amounts to 0.36°C , which gives a mean ‘large-scale’ buoyancy frequency of $N = 1.6 \times 10^{-3} \text{ s}^{-1}$ (≈ 22
165 cycles per day, cpd) using the temperature-density relationship in Fig. 2. This N -value closely
166 corresponds with the mean buoyancy frequency of ~ 20 cpd computed for the same 100 m range from
167 the CTD-profile in Fig. 3d. This gives an approximate mean buoyancy period of $T_N = 2\pi/N = 4000 \text{ s}$.

168 During the first 43 days of the record in mid-summer, no long periods of salinity compensation
169 seem to exist (Fig. 4a). The overview impression is a generally stable stratification in temperature
170 with relatively warmer waters above cooler waters, and some clear exceptions like around day 235.
171 Over time, 2-5 d periodically alternating bands of warmer and cooler waters are observed that are,
172 roughly, uniform in the vertical. In the lower 50 m above the bottom, transitions ('fronts') are visible
173 from relatively warm to cooler waters, e.g. on days 213, 218, 222, 224, 228, Their primary
174 periodicity is thus also some 2-5 d, as observed previously in the Faroe-Shetland Channel (Hosegood
175 and van Haren 2004). Spectra from three different depth levels show no distinct peaks, with largest
176 variance around the sub-inertial frequency $I_{bc} \approx 0.33$ cpd (Fig. 4b). The latter is named after the
177 baroclinic instability modelled by Teigen et al. (2011), and apparently also dominates the appearance
178 of temperature fronts here.

179 Temperature shows no peak around the semidiurnal inertial/tidal band (Fig. 4b). From left to right
180 in this band, main harmonic spectral peaks are expected in the raw periodogram at M_2 , the lunar tidal
181 component, f , the inertial frequency, and S_2 , the solar tidal component. However, none are observed
182 (not shown). We have no information on the local background vorticity, which is assumed zero here.
183 On average, the lunar semidiurnal tidal component is thus outside the band of freely propagating
184 internal gravity waves $f < \sigma < N$, under moderate-strong stratification. However, the entire spectrum is
185 featureless with the lowest energy close to the bottom (blue spectrum) and a more or less constant
186 slope in frequency of σ^{-2} for $\sigma > 13$ cpd = $0.6N$. For about $(0.5-1)f < \sigma < 0.5N$, the spectra roughly
187 slope like σ^{-1} , also for the blue spectrum. Note that the latter changes to a slope of σ^{-3} at about $0.2N =$
188 4.5 cpd, half the local (near-bottom) buoyancy frequency (cf, Fig. 3d).

189 These changes in slope are indicative of a peak in the internal wave's vertical current spectrum of
190 an open ocean internal wave field under sufficient stratification (van Haren 2015). The observed σ^{-2} -
191 slope for $\sigma > N$ into the turbulence band also indicates fine-structure contamination. Accidentally, the
192 extent of this σ^{-2} -slope, both in frequency and variance ranges, and the transition to a weaker σ^{-1} -slope
193 can also be inferred in current meter spectra of Kasajima and Svendsen (2002; their Fig. 2). In fact, of
194 all their seven mooring positions across Fram Strait, the one (station F) nearest to our mooring site

195 shows largest ‘background’ spectral levels. This implies locally relatively high internal wave and
196 turbulence variance levels.

197

198 **3.2 Detailed moored observations**

199 During detailed investigations, many large and thin layers were observed of which a non-
200 exhaustive selection is presented in this Section. In each of the figures, the mean buoyancy period of
201 4000 s is indicated by a purple bar. The colour range is fixed for each figure, but changes are made
202 between the figures for displaying clarity since the mean values vary considerably (cf. Fig. 4a).
203 Isotherm contours are drawn in black; each colour range is divided in 10 equidistant isotherms. Thus,
204 with the varying temperature range, the temperature interval also changes between figures. The
205 ruggedness of isotherms may be used as a qualitative indicator for vertical (diapycnal) turbulent
206 exchange: the more rugged, the more turbulent.

207 The first example shows intrusions, some of which in relatively strong stratification during a
208 general cooling phase of upslope motions (Fig. 5a). The cooler waters from below push the warmer
209 waters up in a not very sharp, but nonetheless turbulent front, or multiple fronts, around day 214.1.
210 Besides the large near-homogeneous layer to the left off the bottom (orange), substantial intrusions
211 are found near the interface (between red and blue). The rightmost intrusion is about 1.2 times longer
212 than the mean buoyancy period. The central intrusion is observed over approximately one buoyancy
213 period. Assuming that we are dealing with a cold intrusion in a warmer environment, its detail (Fig.
214 5b) shows rugged isotherms between the relatively warm (red) waters above and cooler water in the
215 intrusion. This interface would correspond to finger-formation in terms of double diffusion. The
216 interface 5 m below is less rugged, especially in the first half of the period displayed. In terms of
217 double diffusion, this would correspond to a diffusive flux layer. Note that the lower/deeper side of
218 the thin, relatively warm layer below shows very smooth isotherms (the steppiness in the colours
219 reflects the sensor separation of 1 m, which poorly resolves the thinner interface). This calm, weakly
220 turbulent layer delineates a high-frequency quasi-solitary internal wave (dipping at day 214.115). The
221 somewhat deformed yellow layer 10 m below and dipping at day 214.116 seems to become
222 overturned through shear as it is followed 900 s later by a layer in a clearer overturning stage. On a

223 smaller scale, such near-overturning is visible close to the arrow in the rugged part of the intrusion,
224 again suggesting shear-induced turbulence.

225 Also in the warming downslope phase thin (<10 m) and thick (>50 m) layers are observed (Fig.
226 6a). Around day 222.65, a thin warm intrusion is observed separating two cooler water layers of
227 which the colder one (above-left) extends from the near-bottom steeply upward. The upper edge of
228 this thin intrusion is sharply delineated and has the more rugged appearance including small-scale
229 billow-like overturns (Fig. 6b). This is the expected diffusive side of the intrusion. The lower, finger-
230 type side shows smoother isotherms initially up to day 222.65. Later in time, but especially also
231 deeper, more rugged isotherms show larger excursions somehow resembling convective type
232 turbulence. On the large vertical scale of 20-40 m, convective turbulence is observed under a warm
233 descending layer (Fig. 6c). The finger-like turbulence alternate every ~1000 s, and continue in an
234 intrusion around day 223.16. The latter intrusion has a duration that is just shorter than the mean
235 buoyancy period.

236 A more prolonged warm intrusion (Fig. 7a), extending for a day, shows opposite isotherm
237 ruggedness to the one described above: smooth isotherms on its upper, diffusive side, and rugged
238 isotherms on its lower finger side (Fig. 7b). However, the lower side fingers are combined with the
239 presence of Kelvin-Helmholtz (KH) shear-driven overturns, e.g. around days 224.45 and 224.475.
240 Clearer than in Figs 5b and 6b, this 10 m thick intrusion shows blobs or patches of warmer water in its
241 core occurring roughly every 500-1000 s around the highest displacement from the bottom. With
242 them, the intrusion describes a wavy pattern, with a 1000 s periodicity. The following cooling phase
243 shows barely a bottom front, but a cold ‘front-intrusion’ some distance off the seafloor, with rugged
244 isotherms near its lower, diffusive border and smooth isotherms overturning in KH-billows around
245 400 m water depth (day 225.29 in Fig. 7c). This intrusion is also of longer duration than the mean
246 buoyancy scale.

247 A 2.5 h long and wavy filament of warm intrusion is found extending from relatively warm
248 waters into weakly stratified cooler waters, before turbulently ending in (sheared?) currents. This is
249 shown in Figure 8, just prior to the arrival of an intrusive blob of warmer water around day 226.1. The
250 ‘front’ around day 225.95 from which the filament intrudes is similar to the one in Fig. 7c, with more

251 rugged isotherms near the lower border of the cold water (intrusion) and smoother isotherms showing
252 occasional KH-billow overturning near its upper border. The warm intrusion filament (Fig. 8c),
253 similar to the lower border of a front like in Fig. 7c but with the coldest water below, shows fairly
254 smooth isotherms on the upper and lower side, until it starts widening from day 226.03 onward. The
255 upper side waves with a 2000 s period, while the lower side has shorter periods between 400-500 s
256 (indicated by the arrow). That side is more (finger, convective) turbulent too, and seems to dissolve
257 the entire intrusion within an hour after day 226.055.

258 An example of longer lived, larger-scale (>50 m) warm intrusion (with thin cold intrusions inside)
259 is shown in Fig. 9. The intrusion is observed for about a day, and ends around day 236.0 with an
260 apparent front upside down as cooler water moves in from above driven by the following warm
261 waters. This second warm blob also has a relatively thick (>50 m) cold intrusion around day 236.35.
262 The large intrusions are characterized by abundant high-frequency internal waves with periods close
263 to the mean buoyancy period and by smooth isotherms all around them, suggestive of moderate-weak
264 turbulence activity. This contrasts with the rugged isotherms around the slanted intrusion of relatively
265 cold water around day 236.1, which shows 10 m KH-billows (indicated by the arrow) indicative of
266 shear-induced turbulence.

267 In autumn, intrusions of similar thickness variations and temperature fluctuations are observed,
268 albeit bottom front and high-frequency internal wave activity show slightly more often, see the
269 example in Fig. 10. In the 2 d window presented, three distinct small-scale variations are observed.
270 The first (left arrow in Fig. 10a) shows a warm intrusion with rugged isotherms on both its upper and
271 lower sides, with a quasi-periodicity of wavy/finger convection of about 300-600 s (Fig. 10b). This
272 turbulent intrusion occurs after a cold front moving upslope, at some distance but still affecting the
273 bottom. The second (middle arrow in Fig. 10a) follows a bottom front with an interface supporting
274 high-frequency waves in a rank-ordered pattern with largest amplitude and longest period closest to
275 the “cold-front” (Fig. 10c). Note that this front does not represent a highly nonlinear bore, but more a
276 bolus shape. The typical wave-period decreases from about 1500 to 400 s and the amplitude from 10
277 to about 2 m. The former period is very close to the local small-scale buoyancy period (assuming the
278 same temperature-density ratio as before). The latter periods are thus too short to represent freely

279 propagating internal waves. They adopt a nonlinear shape and disintegrate rapidly. Although
280 isotherms above and below are fairly smooth and intrusions are hardly visible, multiple billow-form
281 overturns and sudden nonlinear peak-like waveforms are observed, indicative of convection. The third
282 (right arrow in Fig. 10a) shows smooth small-scale waves observed at the transition from the cooling,
283 upslope to the warming downslope phase (Fig. 10d). Waves having typically 1500 s period,
284 commensurate the local small-scale buoyancy period, also deform a warm intrusion. The latter has
285 very smooth isotherms with shorter scale anomalous temperature (intensity) variations. This
286 resembles much more persistent (for days-weeks) open-ocean observations dominated by larger-scale
287 and linear internal waves (cf. van Haren and Gostiaux 2009). Here, the isotherms surrounding the 40
288 m thick wave-layer show occasional KH-billow overturning (e.g., day 308.34, $z = -390$ m). The train
289 of waves does not exceed 10 wave periods, in contrast with open-ocean observations.

290 An example of upslope moving bore associated with a large-scale N-internal wave is given in Fig.
291 11. The about 60 m high overturning shows similarities with a frontal overturn observed in the tidally
292 dominated methane seep area off New Zealand (van Haren and Greinert 2013): it is identical in height
293 and overturning activity, but it is spread here over a range in time twice as long commensurate the
294 doubling of the buoyancy period. Part of the cold front intrusions may have been formed non-locally,
295 away from the front. The observed frontal wave motions extend to 100 m above the bottom, followed
296 by a layer of intense turbulence also affecting the main pycnocline around $z = -380$ m that is found to
297 widen with time.

298 299 **4 Discussion**

300 The present observations show that above a continental slope intrusions are relatively short-lived.
301 They have durations of maximum a day, more typical a few hours or once-twice the large-scale mean
302 buoyancy period. As this is much shorter than the weeks-months lifetime of intrusions in the open
303 ocean reported previously (e.g., Hebert et al. 1990), nearby boundary effects are expected to be
304 important for the apparent rapid dispersal of intrusions.

1
2 305 Detailed temperature observations show that topography has mixed effects on intrusions. In 1.5 y
3 306 long open-ocean observations around the depth of the lower edge of Mediterranean outflow water in
4 307 the Canary Basin, van Haren and Gostiaux (2009) found intrusions that were persistent for weeks in
5
6 308 the smooth internal waves. However, the intrusions' intensity varied over much shorter time scales of
7
8 309 a few hours to a day. The latter duration is precisely as observed here, while the former is not present
9
10 310 in our data. This implies that the stronger turbulence (on average by a factor of 100 in a tide-
11
12 311 dominated area; van Haren and Gostiaux 2012) above topography compared with the open ocean
13
14 312 reduces the life-time of intrusions to a day or less.
15

16
17 313 Intrusions are suggested to be generated locally, e.g., at fronts between downslope moving warmer
18
19 314 and upslope moving cooler waters. Such 'cold-front-generated' intrusions occur at sub-inertial time-
20
21 315 scales, the main current periodicity here, in the absence of strong tides. The fronts are varyingly
22
23 316 associated with local small-scale near-buoyancy period internal waves, the naturally generated motion
24
25 317 in a stratified fluid upon any forcing, their deformation and eventual breaking. In addition, interior-
26
27 318 generated intrusions are observed to reach the topography from above and mix, typically within a day.
28
29 319 The small-scale blobs of <1 h duration (up to the large-scale buoyancy period) inside intrusions are
30
31 320 also expected being generated by the turbulent processes near the topography.
32
33

34
35 321 Another effect of the internal wave breaking is the abundant generation of shear-induced K-H
36
37 322 billows and convective overturning. This is observed in the loci of rugged and smooth isotherms,
38
39 323 which are found highly variable above and below intrusions thus not reflecting fixed double diffusion
40
41 324 processes. These findings confirm previous microstructure profiler observations from the Yermak
42
43 325 Plateau north of Spitsbergen (Padman and Dillon 1991). In their measurements strong turbulence was
44
45 326 also found in partially salinity-compensated 'quasi-intrusions'.
46
47
48

49 327 Although the present observations are from the Arctic region West of Spitsbergen, where dominant
50
51 328 freely propagating internal tides do not exist, they may be used as examples for other areas where
52
53 329 different water masses are mixed above topography. The appearance of turbulence in most of the
54
55 330 intrusions compared to an open ocean setting suggest a rapid water mass mixing. In the present area,
56
57 331 the precise time-scale and level of turbulence of this mixing of intrusions should be established
58
59 332 through microstructure profiler measurements.
60
61
62
63
64
65

333 Originally, the mooring deployment was also planned to study enhanced mixing processes close to
1
2 334 the seafloor occur. We speculated that methane-charged bottom water in the seep area around 400 m
3
4 335 water depth (Westbrook et al. 2009; Sahling et al. 2014) might be transported higher up into the water
5
6 336 column, possibly across isopycnals that are generally thought to hamper such vertical exchange
7
8
9 337 (Gentz et al. 2014). The observed internal wave-induced turbulent overturning and rapid dispersion of
10
11 338 intrusions might thus have a different impact on methane distribution than expected and could be of
12
13 339 importance for the dispersal of microbial communities. Steinle et al. (2015) relate microbial
14
15 340 methanotrophic activity and community size, important for the oxidation of methane in the waters
16
17 341 around seeps, to physical water mass properties T and S and modeled ocean currents. They show that
18
19 342 cold, in their case bottom-water contains large numbers of aerobic methanotrophs. Our observed
20
21 343 quick dispersion of intrusions would counteract the effect of higher abundances of microbes and their
22
23 344 ability to oxidize more methane in a shorter time. On the other hand, it also serves as good
24
25 345 distribution mechanism for these microbes to be present ‘everywhere at any time’.
26
27
28
29 346

31 347 **Acknowledgments**

32
33 348 We thank captain and crew of R/V Helmer Hanssen for their assistance. We greatly thank M. Laan
34
35 349 for design and construction of NIOZ temperature sensors and assistance in mooring preparation. Data
36
37 350 use requests can be directed to hans.van.haren@nioz.nl.
38
39
40 351

352 **References**

- 1
2 353 Armi L (1978) Some evidence for boundary mixing in the deep ocean. *J Geophys Res* 83:1971-1979
3
4
5 354 Cacchione DA, Drake DE (1986) Nepheloid layers and internal waves over continental shelves and
6
7 355 slopes. *Geo-Mar Lett* 16:147-152
8
9
10 356 Gentz T, Damm E, Schneider von Deimling J, Mau S, McGinnis DF, Schlüter M (2014) A water
11
12 357 column study of methane around gas flares located at the West Spitsbergen continental margin.
13
14 358 *Cont Shelf Res* 72:107-118
15
16 359 Hebert D, Oakey N, Ruddick B (1990) Evolution of a Mediterranean salt lens: scalar properties. *J*
17
18 360 *Phys Oceanogr* 20:1468-1483
19
20
21 361 Holtermann P (2015) Ventilation of the Baltic Sea by lateral intrusions of water masses. 26th IUGG
22
23 362 General Assembly, Praha Cz 22 June-02 July
24
25
26 363 Hosegood P, van Haren H (2004) Near-bed solibores over the continental slope in the Faeroe-
27
28 364 Shetland Channel. *Deep-Sea Res II* 51:2943-2971
29
30
31 365 IOC, SCOR, IAPSO (2010) The international thermodynamic equation of seawater – 2010:
32
33 366 Calculation and use of thermodynamic properties. Intergovernmental Oceanographic
34
35 367 Commission, Manuals and Guides No. 56, UNESCO (English) 196 pp
36
37
38 368 Kasajima Y, Svendsen H (2002) Tidal features in the Fram Strait. *Cont. Shelf Res* 22:2461-2477
39
40 369 May BD, Kelley DE (2001) Growth and steady state stages of thermohaline intrusions in the Arctic
41
42 370 Ocean. *J Geophys Res* 106:16783-16794
43
44
45 371 Munk WH (1966) Abyssal recipes. *Deep-Sea Res* 13:707-730
46
47 372 Padman L, Dillon TM (1991) Turbulent mixing near the Yermak Plateau during the Coordinated
48
49 373 Eastern Arctic Experiment. *J Geophys Res* 96:4769-4782
50
51
52 374 Perkin RG, Lewis EL (1984) Mixing in the West Spitsbergen Current. *J Phys Oceanogr* 14:1315-1325
53
54 375 Ruddick B (1984) A practical indicator of the stability of the water column to double-diffusive
55
56 376 activity. *Deep-Sea Res A* 30:1105-1107
57
58
59
60
61
62
63
64
65

1 377 Ruddick B (1992) Intrusive mixing in a Mediterranean salt lens: Intrusion slopes and dynamical
2 378 mechanisms. *J Phys Oceanogr* 22:1274-1285
3
4 379 Rudnick DL, Ferrari R (1999) Compensation of horizontal temperature and salinity gradients in the
5
6 380 ocean mixed layer. *Science* 283:526-529
7
8
9 381 Sahling H, et al. (2014) Gas emissions at the continental margin west off Svalbard: mapping,
10
11 382 sampling, and quantification. *Biogeosci* 11:7189-7234.
12
13
14 383 Schauer U, Fahrbach E, Østerhus S, Rohardt G (2004) Arctic warming through the Fram Strait:
15
16 384 Oceanic heat transport from 3 years of measurements. *J Geophys Res* 109:C06026,
17
18 385 doi:10.1029/2003JC001823
19
20
21 386 Schmitt RW (1999) Spice and the demon. *Science* 283:498-499
22
23 387 Steinle L, et al. (2015). Water column methanotrophy controlled by a rapid oceanographic switch.
24
25 388 *Nature Geosci* 8:378-382, DOI: 10.1038/NGEO2420
26
27 389 Teigen SH, Nilsen F, Skogseth R, Gjevik B, Beszczynska-Möller A (2011) Baroclinic instability in
28
29 390 the West Spitsbergen Current. *J Geophys Res* 116:C07012, doi:10.1029/2011JC006974
30
31
32 391 Turner JS (1979) Buoyancy effects in fluids. Cambridge University Press 368 pp
33
34 392 van Haren H (2015) A composite vertical current spectrum for strongly and weakly stratified seas and
35
36 393 oceans. *J Mar Res* 73:33-48
37
38
39 394 van Haren H, Gostiaux L (2009) High-resolution open-ocean temperature spectra. *J Geophys Res*
40
41 395 114:C05005, doi:10.1029/2008JC004967
42
43 396 van Haren H, Gostiaux L (2012). Detailed internal wave mixing observed above a deep-ocean slope. *J*
44
45 397 *Mar Res* 70 :173-197
46
47
48 398 van Haren H, Greinert J (2013) Variability of internal frontal bore breaking above Opouawe Bank
49
50 399 methane seep area (New Zealand). *Geochem Geophys Geosys* 14:2460-2473,
51
52 400 doi:10.1002/ggge.20170
53
54 401 van Haren H, Laan M, Buijsman D-J, Gostiaux L, Smit MG, Keijzer E (2009) NIOZ3: independent
55
56 402 temperature sensors sampling yearlong data at a rate of 1 Hz. *IEEE J Ocean Eng* 34:315-322
57
58
59
60
61
62
63
64
65

403 Westbrook GK, et al. (2009) Escape of methane gas from the seabed along the West Spitsbergen
1 continental margin. *Geophys Res Lett* 36:L15608, doi:10.1029/2009GL039191.
2
3
4 405
5
6 406
7
8
9
10
11
12
13
14
15
16
17
18
19
20
21
22
23
24
25
26
27
28
29
30
31
32
33
34
35
36
37
38
39
40
41
42
43
44
45
46
47
48
49
50
51
52
53
54
55
56
57
58
59
60
61
62
63
64
65

407 **Fig. 1.** Svalbard with mooring location indicated by the red dot. The nearest CTD location was 1 km
1
2 408 to the SW of the mooring.
3

4 409
5
6 410 **Fig. 2.** Temperature-density relationship from CTD-observations for the lower 150 m above the
7
8 411 bottom, at 1 km to the SW of the mooring. The linear best-fit is given (see text).
9

10 412
11
12
13 413 **Fig. 3.** CTD observations made shortly before mooring recovery, at a site 1 km to the SW and slightly
14
15 414 deeper than the mooring. (a) Density anomaly, referenced to 400 m. (b) Conservative temperature.
16
17 The vertical bar indicates the range of moored temperature sensors. (c) Absolute salinity. The x-
18 415 axis scale is similar to the temperature-scale in panel b in the sense of equivalent contribution to
19
20 416 density variations. (d) Buoyancy frequency, averaged over 10 m vertical intervals. The vertical
21
22 417 dashed line indicates the average N-value estimated from mean moored temperature observations
23
24 418 using the temperature-density relationship from Fig. 2.
25
26 419
27
28

29 420
30
31 421 **Fig. 4.** Overview of the first 43 days of moored high-resolution temperature sensor observations
32
33 422 above the continental slope West of Svalbard. (a) Time-depth series of Conservative Temperature.
34
35 423 (b) Spectra of the upper, middle and lowest sensors, weakly smoothed to provide approximately 15
36
37 degrees of freedom. The local mean buoyancy frequency is indicated together with its approximate
38 424 spread (cf., Fig. 3d). Three spectral slopes σ^{-x} , $x = 1, 2, 3$ are indicated (see text). I_{bc} indicates the
39
40 425 central frequency for topographic baroclinic instabilities modelled by Teigen et al. (2011).
41
42 426
43
44 427
45

46 428 **Fig. 5.** Example of detail observations of intrusions in a relatively strongly stratified layer. Ten black
47
48 contours are drawn, equally distributed over the displayed temperature range. The purple bar
49 429 indicates the duration of one mean buoyancy period of 4000 s. (a) Six hour time-depth series of
50
51 430 Conservative Temperature. (b) One-hour detail zoom near arrow in a.
52
53 431
54
55 432
56
57

58 433 **Fig. 6.** As Fig. 5, but for intrusions in near-homogeneous layers. Note the different temperature range,
59
60 434 and hence the different interval between temperature-contours. (a) Thirty hour time-depth series of
61
62
63
64
65

435 Conservative Temperature. (b) One-and-a-half hour detail of thin layer intrusion near left arrow in
1
2 436 a. (c) Three-and-a-half hour detail of finger-like convection and thick layer intrusion around right
3
4 437 arrow in a.
5

6 438
7
8
9 439 **Fig. 7.** As Fig. 5, but for a long, relatively thin intrusion in near-homogeneous waters. Note the
10
11 440 slightly different temperature range. (a) Thirty hour time-depth series of Conservative
12
13 441 Temperature. (b) Two-and-a-half hour around highest point of intrusion, as indicated by left arrow
14
15 442 in a. (c) Nearly three hours of quasi-front intrusion, near right arrow in a.
16

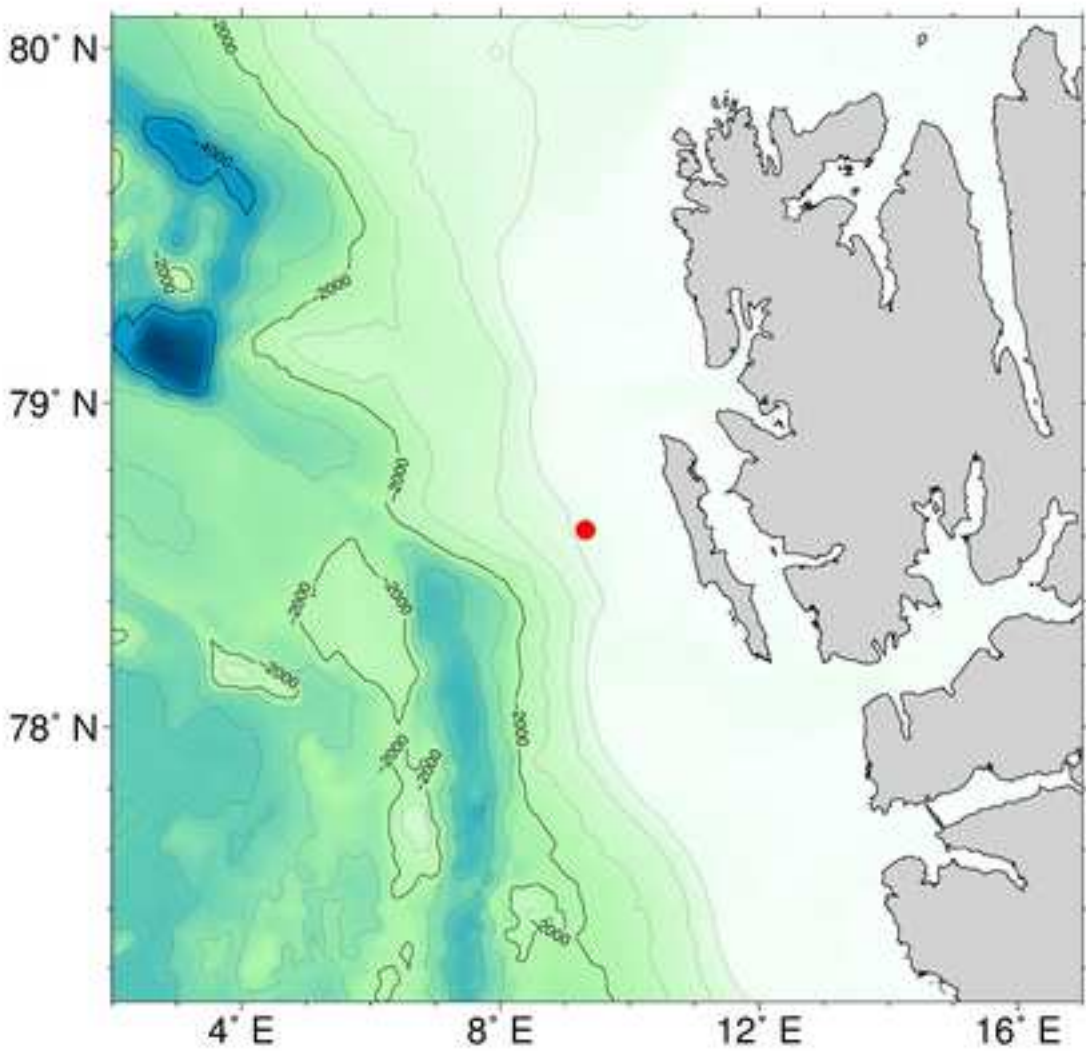
17 443
18
19
20 444 **Fig. 8.** As Fig. 5, but for long-thin filament and larger-scale ‘blob’ intrusions in near-homogeneous
21
22 445 waters. Note the slightly different temperature range. (a) Eight hour time-depth series of
23
24 446 Conservative Temperature. (b) Forty minute detail of ‘quasi-front’ intrusion near arrow in a. (c)
25
26 447 Two hour detail of thin filament with high-frequency internal wave oscillation having half-hour
27
28 448 periodicity around day 226.04.
29

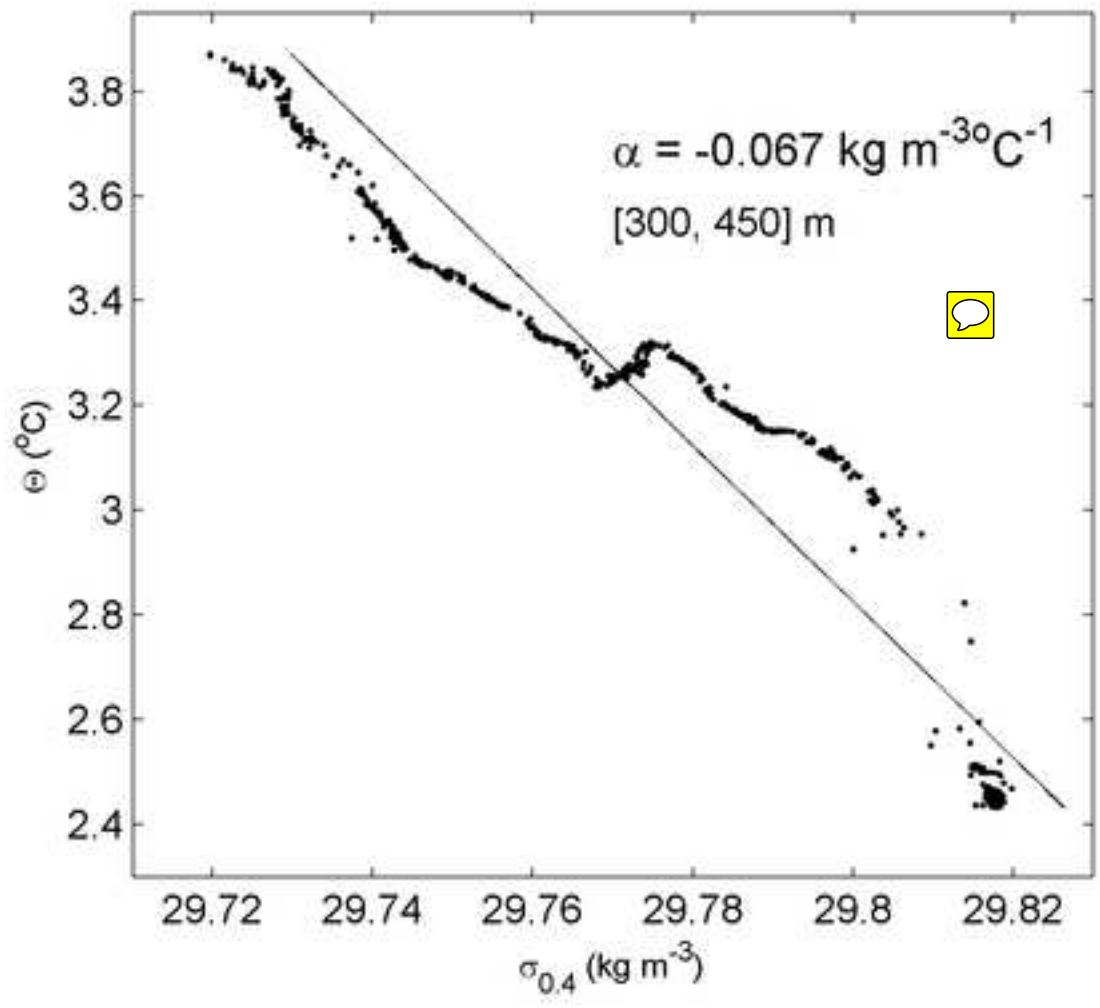
30 449
31
32
33 450 **Fig. 9.** As Fig. 5, but for twenty-nine hour time-depth series of Conservative Temperature showing an
34
35 451 example of a thick-layer intrusion (orange area) with thin-layers inside and bottom fronts with high-
36
37 452 frequency internal waves, and a slant intrusion (blue area) with Kelvin-Helmholtz billows near the
38
39 453 arrow. Note the different temperature range.
40

41 454
42
43
44 455 **Fig. 10.** As Fig. 5, but for fronts and intrusions in late fall with three 3 hour detail panels. Note the
45
46 456 different temperature range. (a) Two day time-depth overview of Conservative Temperature. (b)
47
48 457 Turbulent intrusion near left arrow in a. (c) After bottom-front passage with high-frequency
49
50 458 internal waves having 30-15 min periodicity near middle arrow in a. (d) Around change into the
51
52 459 warming phase with high-frequency internal waves having 25 min periodicity near right arrow in a.
53

54 460
55
56
57
58 461 **Fig. 11.** As Fig. 5, but for large-scale buoyancy period wave upon a cold front in 7 h and 4000 s
59
60 462 (length purple bar) panels. Note the change in colour, time and depth ranges.
61
62
63
64
65

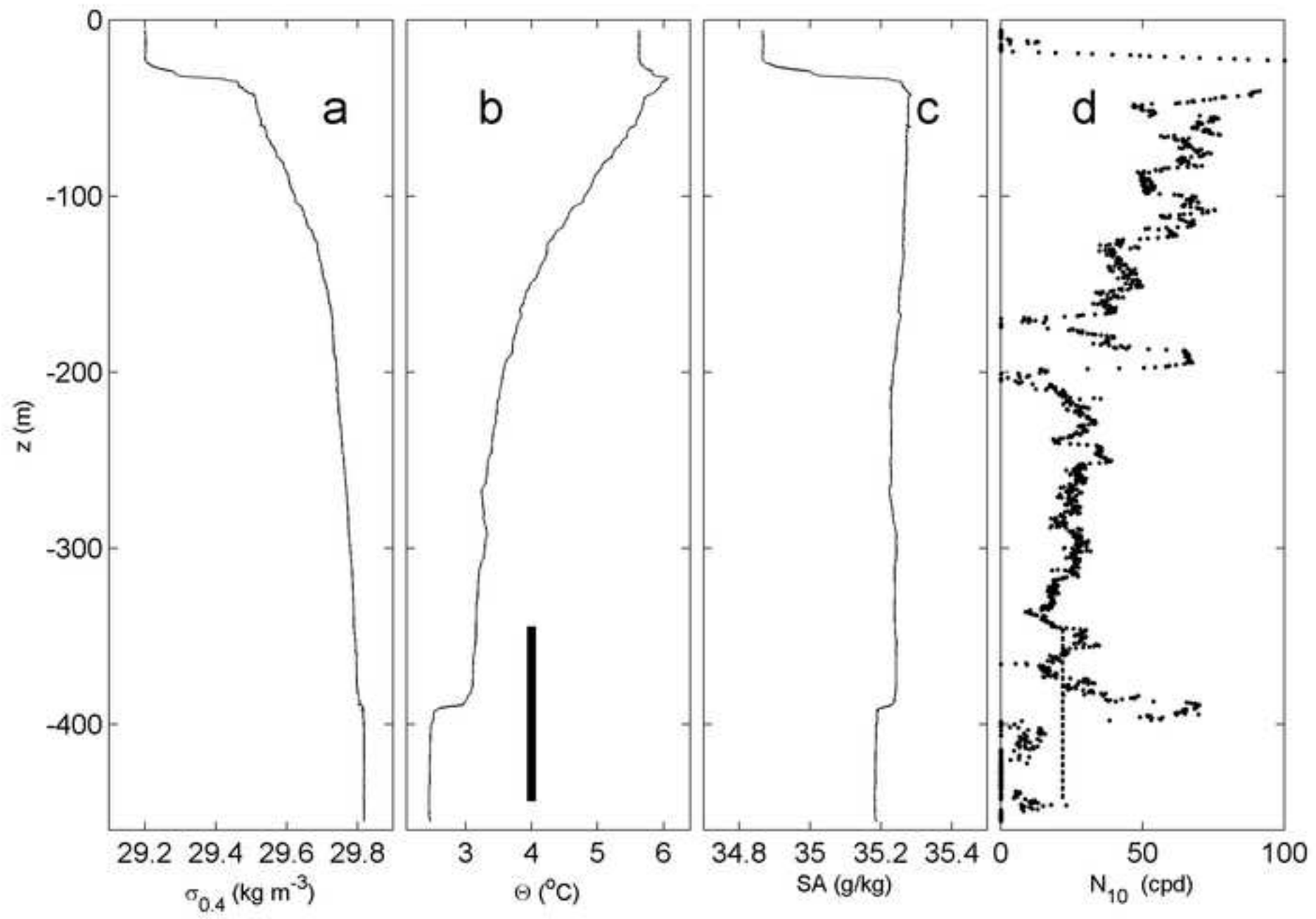
1
2
3
4
5
6
7
8
9
10
11
12
13
14
15
16
17
18
19
20
21
22
23
24
25
26
27
28
29
30
31
32
33
34
35
36
37
38
39
40
41
42
43
44
45
46
47
48
49
50
51
52
53
54
55
56
57
58
59
60
61
62
63
64
65

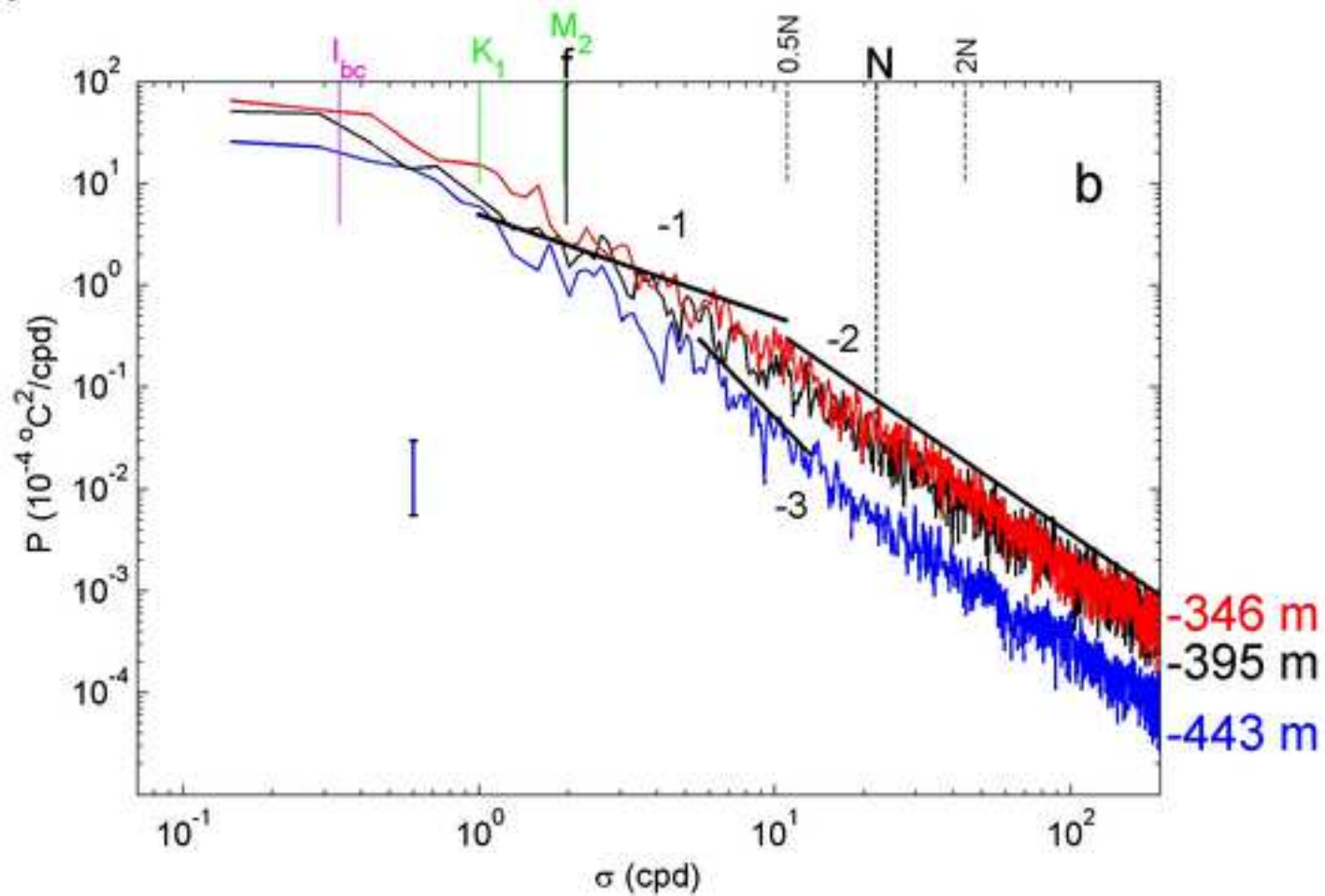
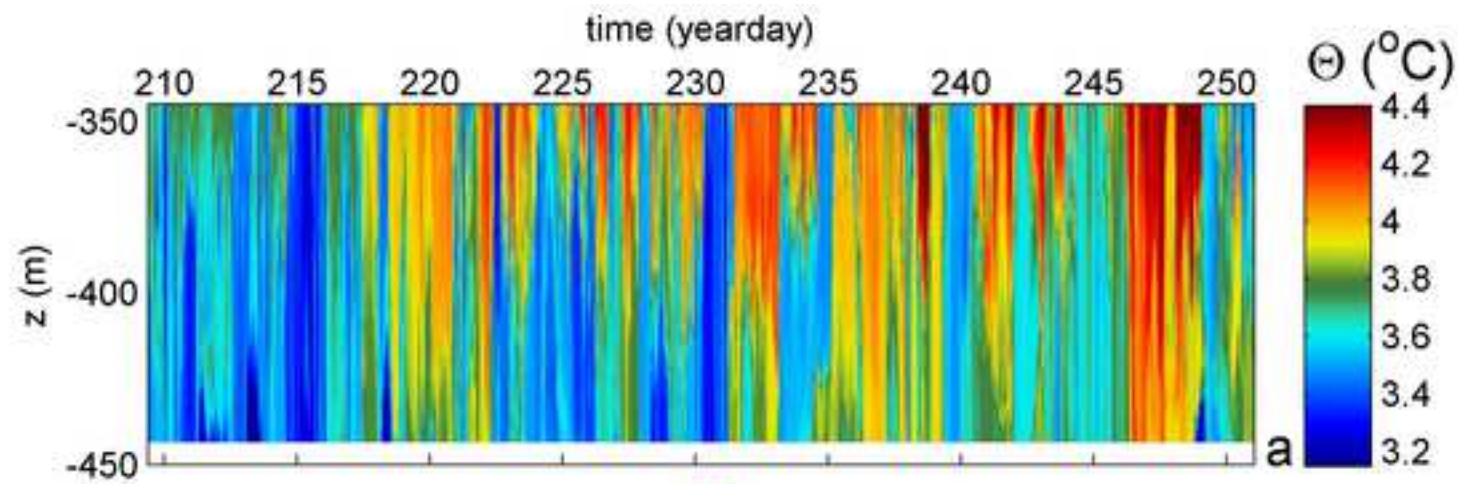


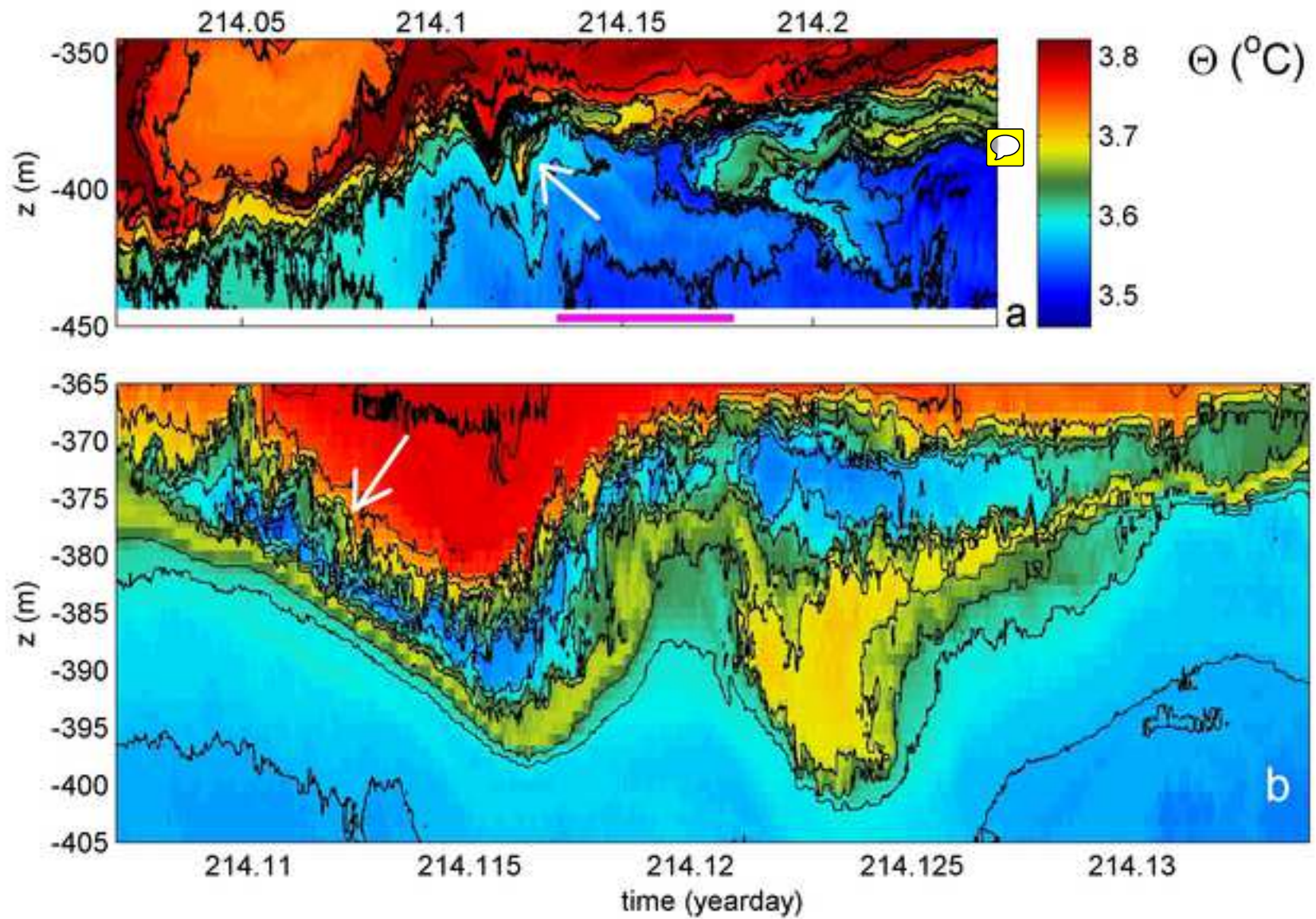


1
2
3
4
5
6
7
8
9
10
11
12
13
14
15
16
17
18
19
20
21
22
23
24
25
26
27
28
29
30
31
32
33
34
35
36
37
38
39
40
41
42
43
44
45
46
47
48
49

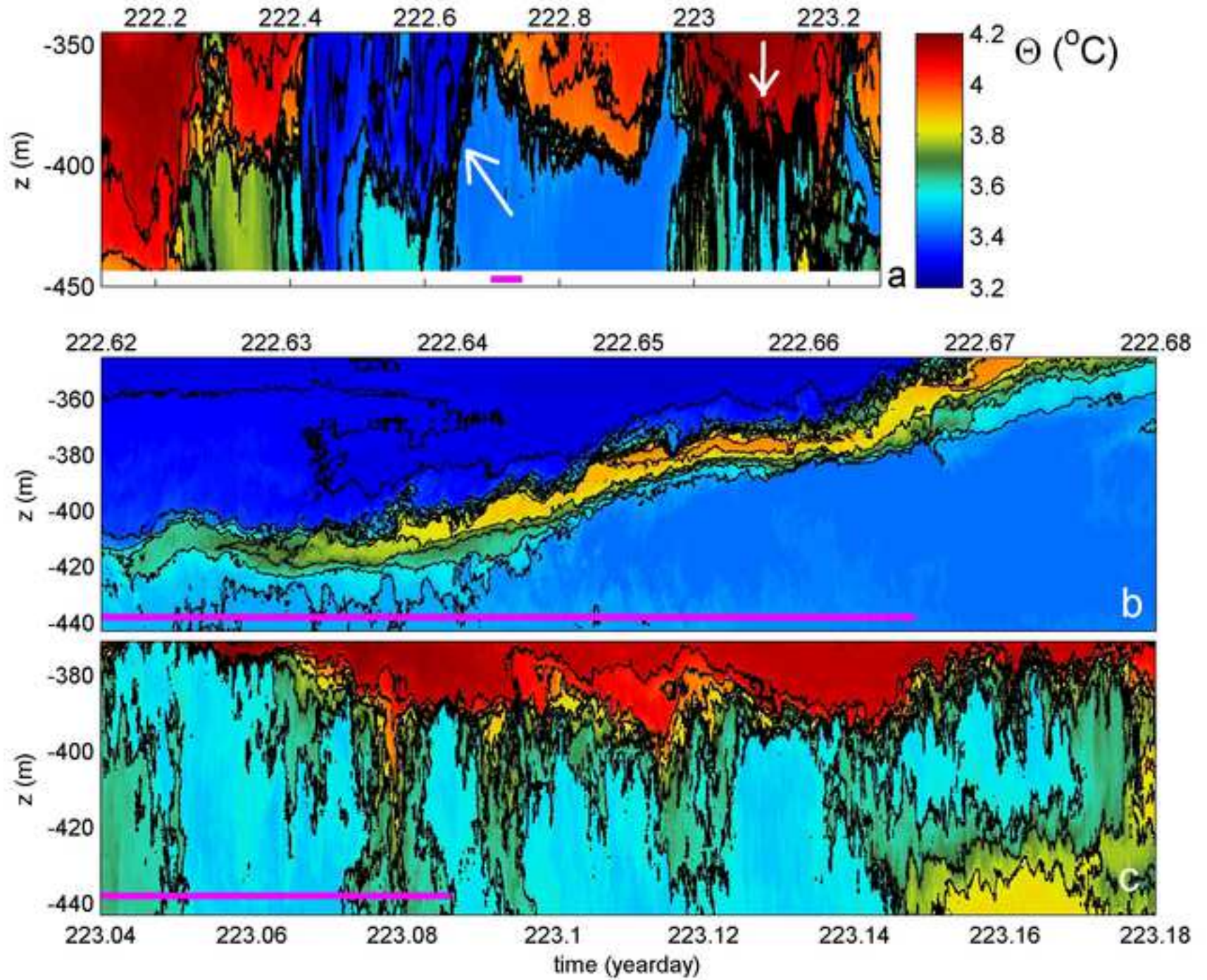
1
2
3
4
5
6
7
8
9
10
11
12
13
14
15
16
17
18
19
20
21
22
23
24
25
26
27
28
29
30
31
32
33
34
35
36
37
38
39
40
41
42
43
44
45
46
47
48
49



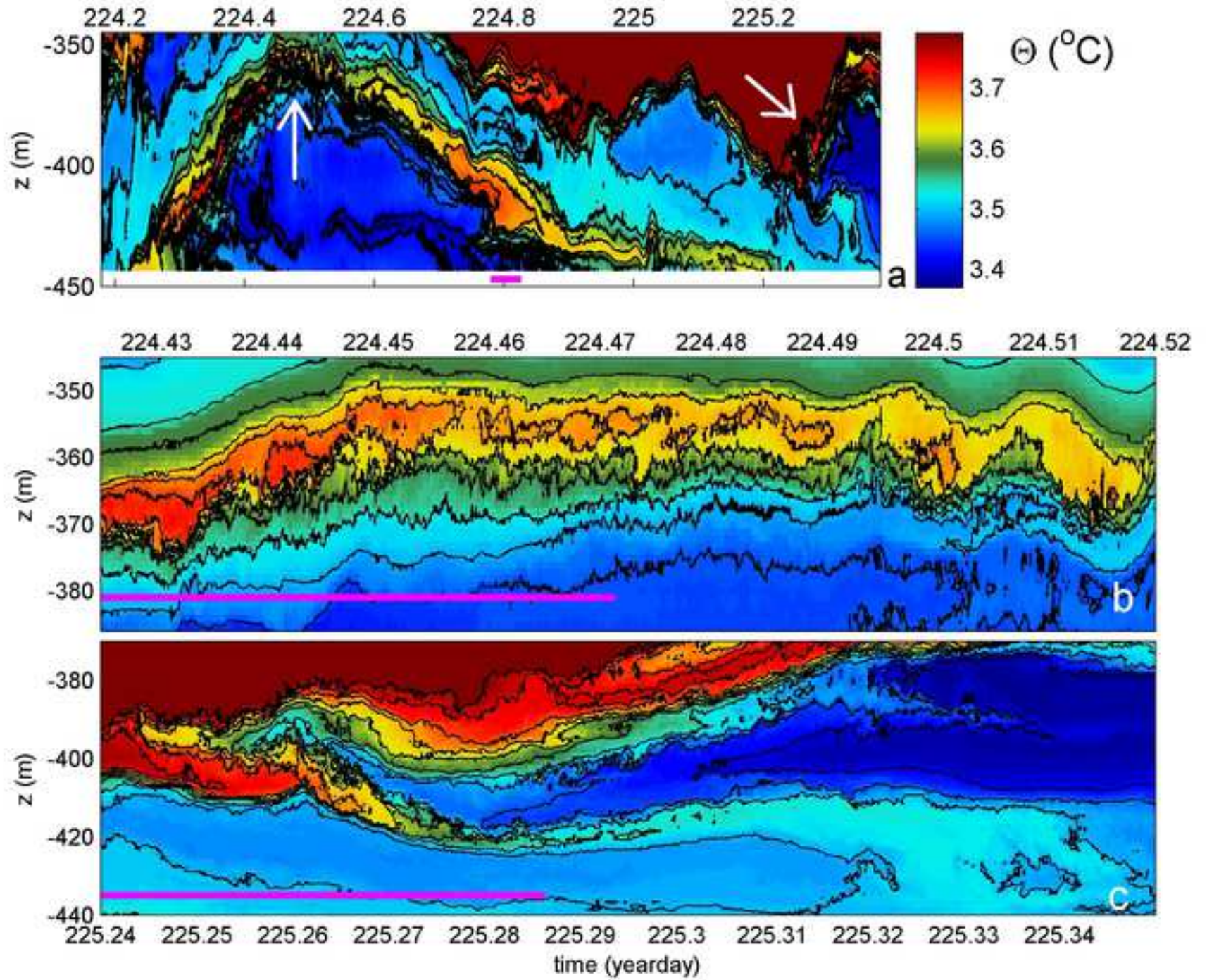


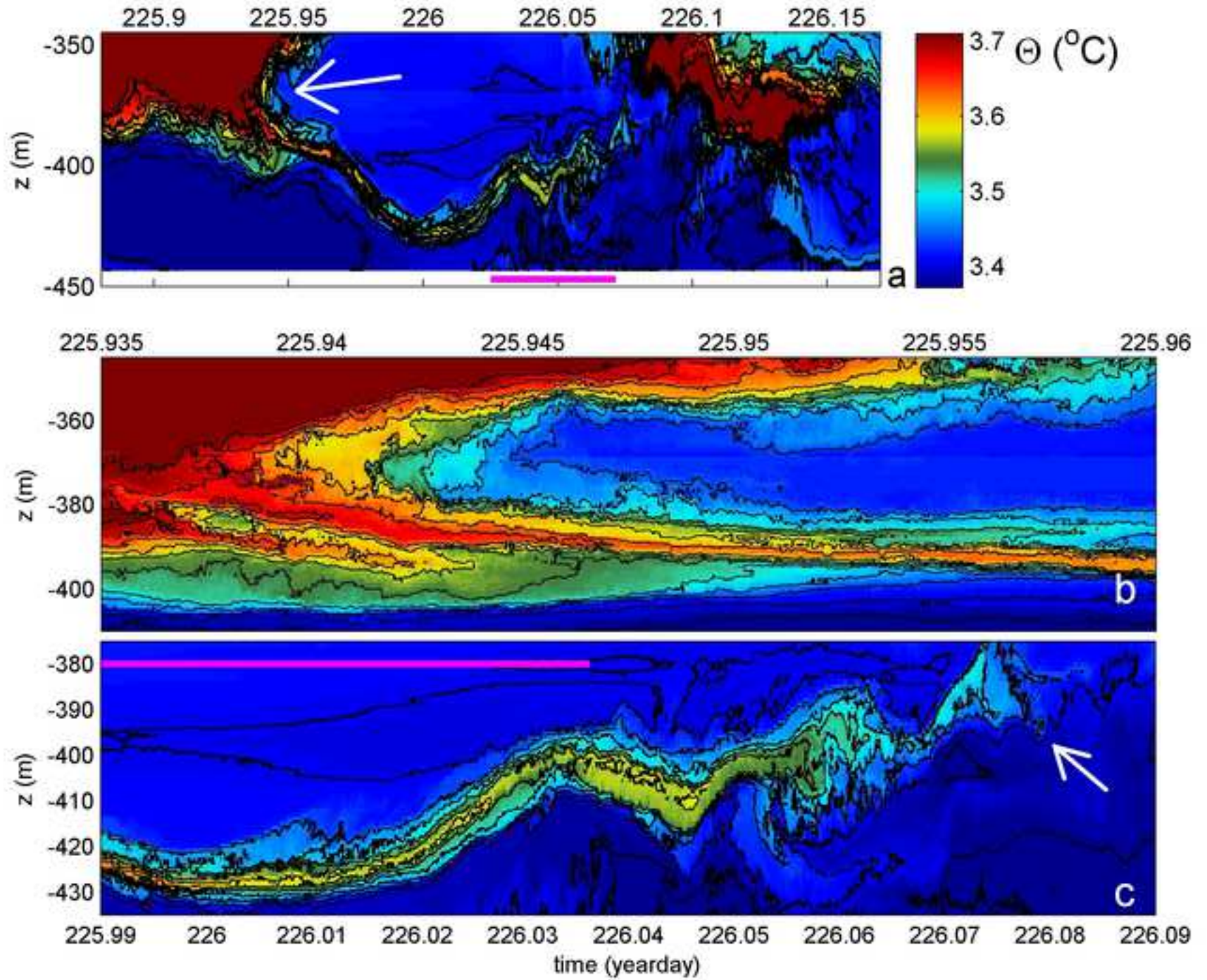


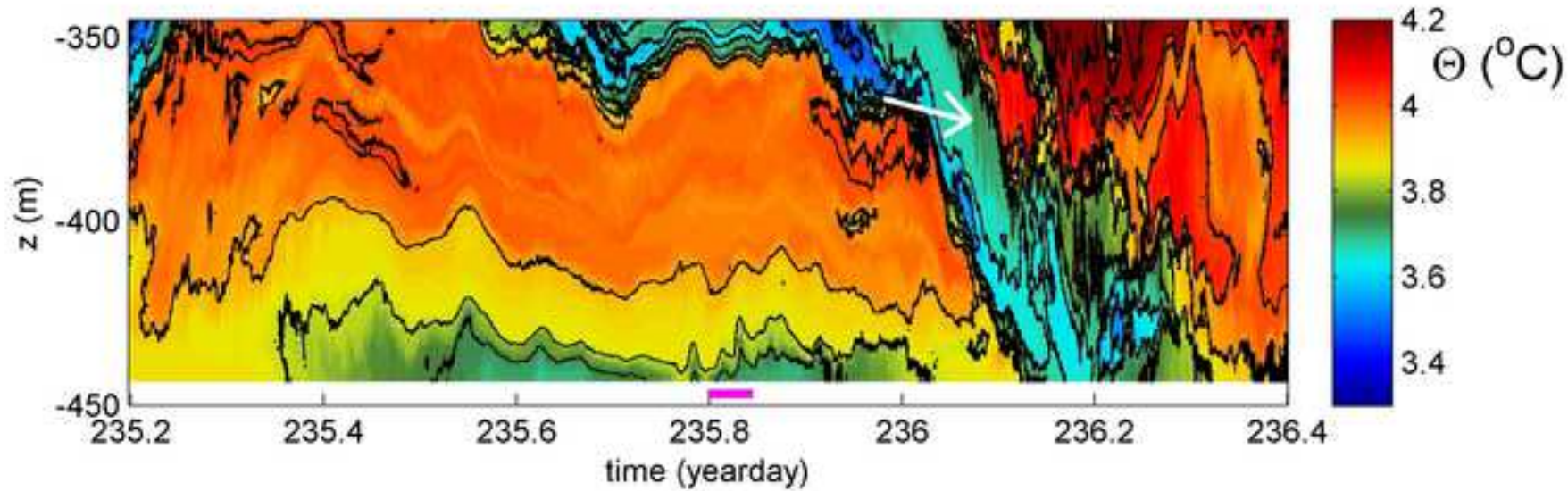
1
2
3
4
5
6
7
8
9
10
11
12
13
14
15
16
17
18
19
20
21
22
23
24
25
26
27
28
29
30
31
32
33
34
35
36
37
38
39
40
41
42
43
44
45
46
47
48
49



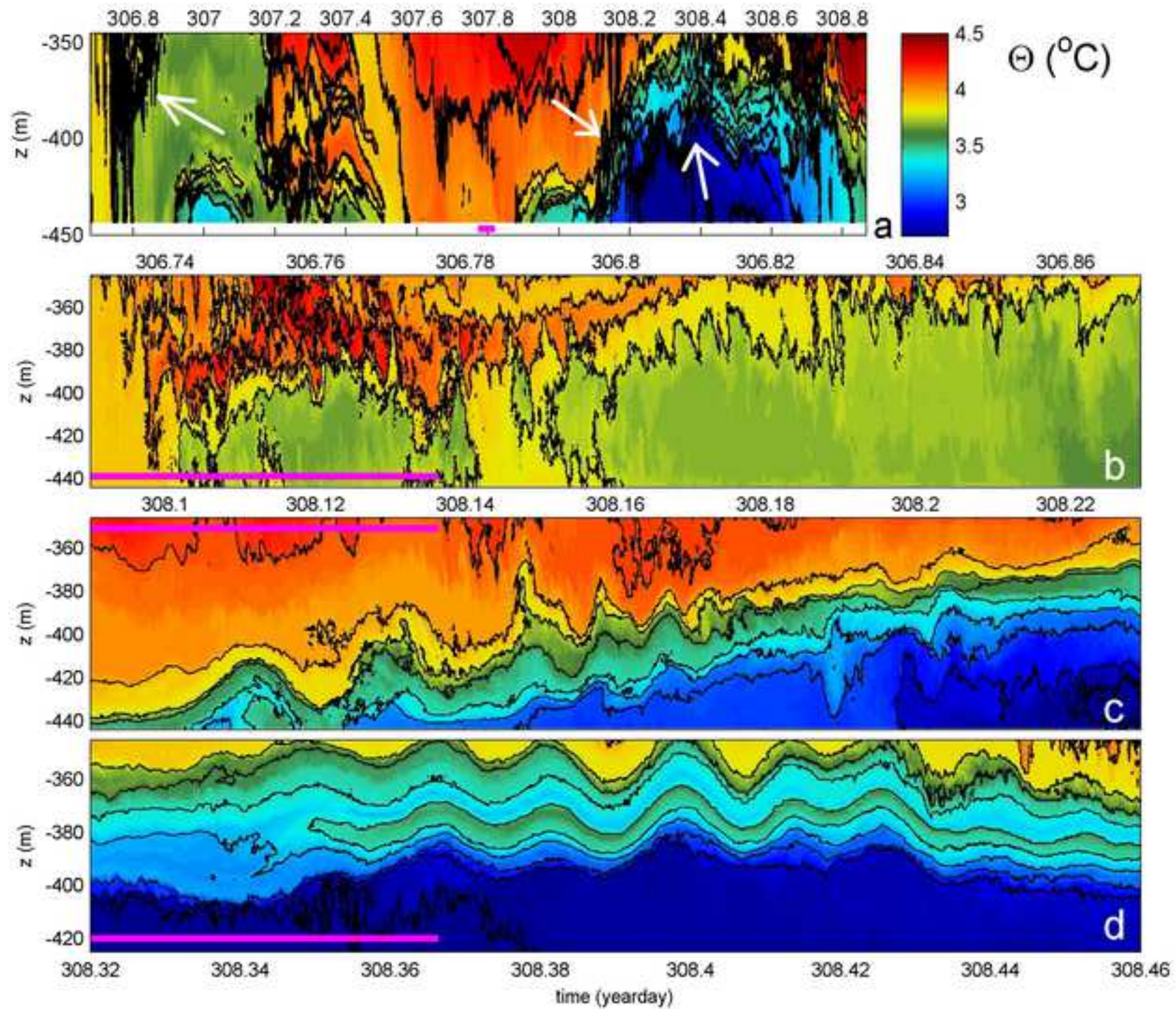
1
2
3
4
5
6
7
8
9
10
11
12
13
14
15
16
17
18
19
20
21
22
23
24
25
26
27
28
29
30
31
32
33
34
35
36
37
38
39
40
41
42
43
44
45
46
47
48
49



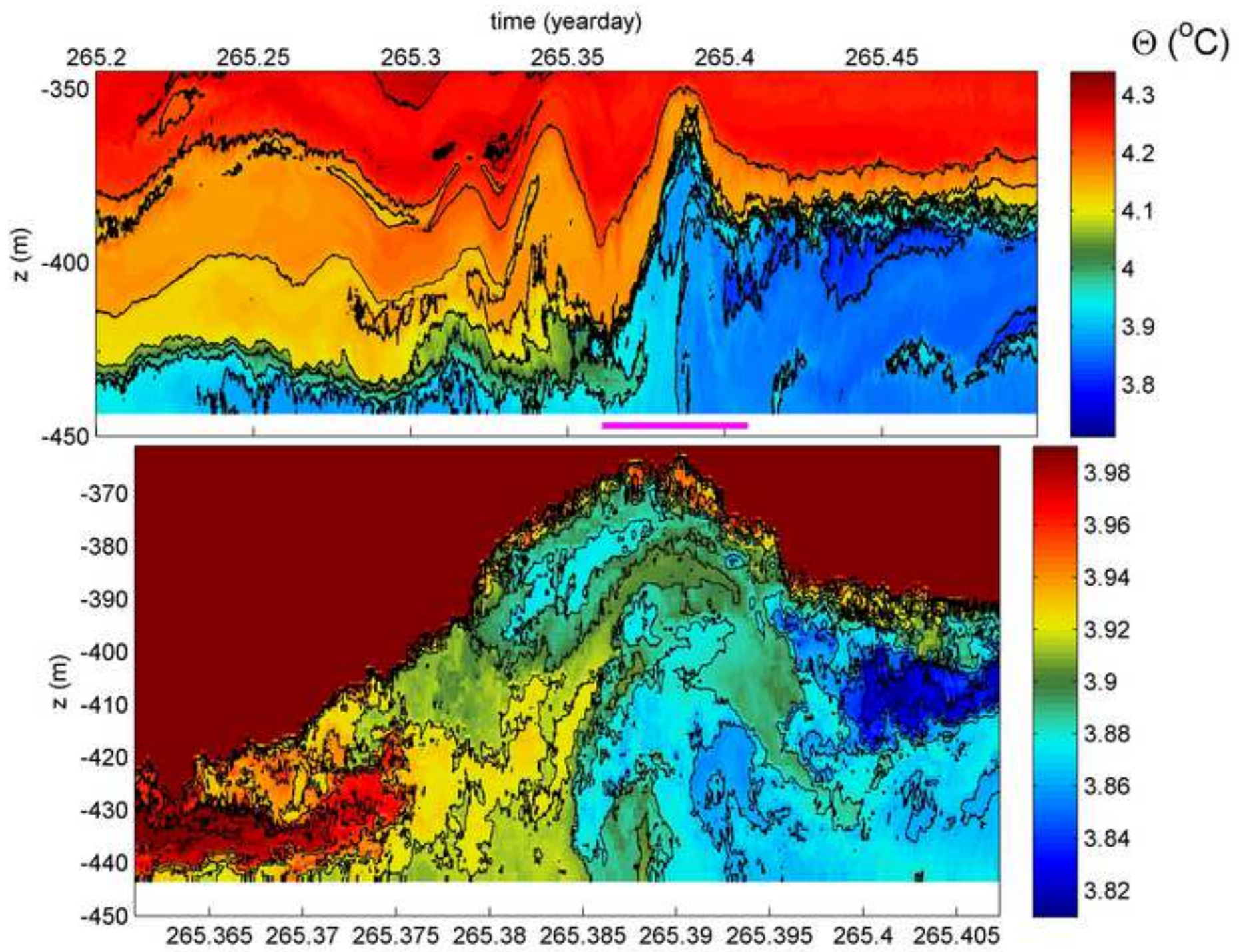




1
2
3
4
5
6
7
8
9
10
11
12
13
14
15
16
17
18
19
20
21
22
23
24
25
26
27
28
29
30
31
32
33
34
35
36
37
38
39
40
41
42
43
44
45
46
47
48
49



1
2
3
4
5
6
7
8
9
10
11
12
13
14
15
16
17
18
19
20
21
22
23
24
25
26
27
28
29
30
31
32
33
34
35
36
37
38
39
40
41
42
43
44
45
46
47
48
49



1
2
3
4
5
6
7
8
9
10
11
12
13
14
15
16
17
18
19
20
21
22
23
24
25
26
27
28
29
30
31
32
33
34
35
36
37
38
39
40
41
42
43
44
45
46
47
48
49